Tribol Lett (2017)65:48
DOI 10.1007/s11249-017-0832-x

METHODS PAPER

On Stress-Induced Tribochemical Reaction Rates

Wilfred Tysoe[1]

Received: 12 January 2017 / Accepted: 27 February 2017

Abstract A number of recent experiments have demonstrated that normal and shear stresses are able to accelerate the rates of chemical reactions of adsorbates on surfaces, yielding an approximately exponential increase in reaction rate with force. It seems that such mechanochemical reactions play a central role in tribochemistry and the consequent formation of anti-wear or friction-reducing films from lubricant additives. It is thus appropriate to summarize the theories that can be used to analyse such tribochemical data. The models have a strong parallel with those used to analyse sliding friction, the Prandtl/Tomlinson model. It is found that the force-dependent activation barrier for chemical reactions varies as $E_{act}(F) = E_{act} + AF + BF^2$. The linear variation in activation barrier with force, the so-called Bell equation, and the quadratic dependence, the so-called Hammond effect, are analysed using model reaction energy profiles, which reveal a dependence of the parameters A and B on the shape of the energy profile. The influence of contact pressure and sliding velocity is also discussed. The above models assume that the normal and shear stresses are coplanar with the thermal reaction coordinate for the tribochemical processes, and the effects of this not being the case are also discussed. Finally, the existing results of tribochemical reactions of oxygen-functionalized graphene and zinc dialkyl dithiophosphates are also analysed using these models.

✉ Wilfred Tysoe
wtt@uwm.edu

[1] Department of Chemistry and Biochemistry, University of Wisconsin-Milwaukee, Milwaukee, WI 53211, USA

Keywords Tribochemistry · Bell model · Extended-Bell model · Hammond effect · Oxygen-functionalized graphene · Zinc dialkyl dithiophosphates (ZDDP)

1 Introduction

Modern lubricants are generally quite complex and incorporate a wide range of compounds including antioxidants, detergents, corrosion inhibitors, anti-foaming agents and viscosity index improvers, as well as those that react at the sliding interface to form friction- or wear-reducing films [1]. Friction- and wear-reducing additives often contain elements such as sulphur, phosphorus or halogens [2] that react at the sliding interface to form a "tribofilm". The interfacial chemistry often differs considerably from the thermal chemistry, and various effects have been invoked to rationalize the differences including the presence of local "flash temperatures" [3], the emission of electrons during sliding [4] or high contact pressures [5]. While the high interfacial temperature induced by sliding is responsible for tribofilm formation, in particular in the so-called extreme-pressure regime [6, 7], it is becoming increasingly clear that a direct mechanochemical coupling of an external force that accelerates the reaction rate [8–16] plays an important role in tribochemistry. This idea has proven challenging to verify because of the difficulty in designing experiments in which other effects, such as the high local, transient energy input that occurs when asperities at the interface slide over each other, do not contribute. This energy input is characterized by a flash temperature, but may not be a temperature in the true thermodynamic meaning since the interface during sliding need not necessarily be in thermal equilibrium [17]. In addition, it is often challenging to accurately calculate flash temperatures

Published online: 09 March 2017

[18–20] making it difficult to establish whether local frictional heating, or some other effect, is responsible for tribochemical behaviour.

However, recent experiments under conditions where the interfacial temperature rise was carefully controlled have provided compelling evidence that direct mechanical coupling of the external force to the surface chemical reaction is responsible for, at least some, tribochemistry. For example, recent atomic force microscopy (AFM) experiments, in which the contact conditions are sufficiently mild that the above effects can be excluded, have demonstrated that interfacial shear and pressure can accelerate the rate of tribofilm formation from zinc dialkyl dithiophosphate (ZDDP), [21] one of the oldest anti-wear oil additives [22]. This was recently confirmed at a more macroscopic scale by carrying out experiments with ZDDP dissolved in high-internal-friction base oils that sustained high shear forces, but prevented direct solid–solid contact [23]. This paper also pointed out that invoking shear effects could potentially explain some enigmas surrounding anti-wear film formation from ZDDP. It has also been shown that interfacial shear can induce adsorbate decomposition [24–26] and demonstrated that the reaction rate increases approximately exponentially with shear stress [21, 23, 24]. It is thus appropriate to discuss the theoretical basis for analytical models for stress-assisted surface chemical reaction kinetics and their difficulties and limitations and to provide approaches for extracting parameters from measurements of tribochemical reaction rates as a function of shear stress and/or contact pressure that will provide stringent tests of such models. It is noted that recent nanoscale wear experiments have shown similar exponential increases in wear rate with shear stress [27], so that such wear processes could be viewed as a type of chemical reaction. However, since the exact transformation occurring during these processes is not well defined, they will be excluded from the following discussion.

2 Background

The existence of a potential energy surface is central to analysing chemical reaction kinetics and dynamics. This describes the potential energy (arising by virtue of the positions of the atoms) of a system of atoms as a function of the positions $\underline{r}_i$ of the i^{th} atom, $V(\underline{r}_i)$, due to the various types of interactions, ionic, chemical bonding, van der Waals etc., between them. It is often referred to as a Born–Oppenheimer potential energy surface since its calculation is based on the Born–Oppenheimer approximation; this essentially assumes that electrons, which are very much lighter than nuclei, can move almost instantaneously in response to the much slower nuclear motion. This approximation allows the nuclear and electronic motions to be calculated separately.

Local minima in this multi-dimensional potential energy surface correspond to locally stable configurations, where the atomic coordinates at these local minima describe the structure of the system. Local dynamics, such as molecular vibrations are analysed by considering the forces acting on the atoms, which is calculated from the gradient of the potential ($\underline{F} = -\underline{\nabla} V$) and by solving the equations of motion. This is often carried out for complex atomic systems by solving the classical Newton's laws of motion for a parameterized potential energy surface for relatively small deviations from the minima using so-called molecular dynamics (MD) simulations [28].

The average energy of the atoms increases in proportion to the absolute temperature T, with a distribution of energies given by the Boltzmann distribution. In this case, the probability of an atom having an energy between E and $E + \mathrm{d}E$, $P(E)\mathrm{d}E$ is given by $P(E)\mathrm{d}E \sim \exp\left(-\frac{E}{k_{\mathrm{B}}T}\right)\mathrm{d}E$, where k_{B} is the Boltzmann constant. Thus, as the temperature T increases, the proportion of the system that has sufficient energy to surmount an energy barrier between one minimum in the potential energy surface and another, known as the activation energy, E_{act}, increases. This probability is proportional to: $\int_{E_{\mathrm{act}}}^{\infty} \exp\left(-\frac{E}{k_{\mathrm{B}}T}\right)\mathrm{d}E \propto \exp\left(-\frac{E_{\mathrm{act}}}{k_{\mathrm{B}}T}\right)$. Because of the exponential dependence on the height of the activation energy barrier, the transition from one to another energy minimum will occur with the highest probability via the lowest energy pathway between the two. This enables this complex, multi-dimensional problem to be significantly simplified by considering only the lowest-energy pathways and ignoring all the rest. Thus, the problem can be analysed by just considering the potential energy profile along these lower-energy pathways, by plotting the free energy versus the so-called reaction coordinate, which describes how the positions of the atoms evolve as the system energy changes from the initial energy minimum, passes over the lowest energy maxima (which are saddle points), to the final states. In practice, the rates of thermal reactions do not depend critically on the shape of the energy profiles, merely the height of the energy barrier relative to the initial state. This is not the case for mechanically induced reactions.

Within this simplified model, the rate at which the system transits the energy barrier is proportional to $\exp\left(-\frac{E_{\mathrm{act}}}{k_{\mathrm{B}}T}\right)$, and rates of chemical reactions have been found to quite accurately follow this so-called Arrhenius behaviour [29]. The configuration of the atoms in the system at the peak of the energy barrier, known as the

transition state, is called the activate complex, and reaction kinetics can be analysed in detail by this model (known as transition-state theory), proposed by Eyring [30]. Here, statistical thermodynamics is used to calculate an equilibrium constant between the initial and transition state, and thereby calculate the transition-state population by assuming that it is in equilibrium with the initial state [31]. The rate of product formation is then taken to be proportional to the population in the transition state. This, in principle, allows the pre-exponential factor, A in front of the Arrhenius term, $\exp\left(-\frac{E_{\text{act}}}{k_{\text{B}}T}\right)$, to be calculated, but this is often challenging. The value of the activation energy, however, can be calculated using quantum theory [32, 33].

In transition-state theory, the initial (reactant) state is invariably at a local energy minimum, so that the local potential energy surface has a positive curvature, while the transition state is a saddle point, which has negative curvature in a direction along the reaction coordinate, but can have positive curvatures perpendicular to it. As will be seen later, this can have implications for the tribochemical behaviour.

The effect of an external force is to influence and, in general, decrease the height of the activation barrier. This has the effect of increasing the rate of thermally activated transitions over this barrier with a consequent increase in the reaction rate; the reaction is still thermally activated and depends on temperature. The physical concept behind describing the influence of an external force on lowering the activation barrier is straightforward; the external force can effectively push the system from its initial energy minimum towards the activation barrier so that the energy barrier is reduced by the amount of work done on the system. In the case of constant-force sliding, this work is $\underline{F} \cdot \underline{r}$, where $\underline{F}$ is the force and $\underline{r}$ is the distance moved. In the case of compliant sliding, for example, by an AFM tip, the work is $^1/_2 k(X-x)^2$, where X is the position of the cantilever with force constant k, and x the tip position. In the following, we shall focus on the most commonly used constant-force sliding.

In this case, the direction of the force exerted on the system relative to the potential energy surface can have a profound effect. Experimentally, this force can be applied in tension, where one end of the chemical system is anchored, while the other end is pulled. This can either be a bulk sample or a single molecule, and this regime is a major focus of mechanochemistry [16, 34–38]. Alternatively, the external force can be applied at a surface and consists of normal and shear forces. This method of applying forces to induce tribochemistry is the focus on this paper, although the general principles apply equally well to both regimes.

While, as emphasized above, the tribochemical behaviour depends on the way in which the applied force is aligned with respect to the potential energy surface, it is common to use models in which the force is taken to act within the plane that defines the reaction coordinate. This has the advantage of being conceptually simple since plots of activation energy are well understood for thermal reactions. It is also the approach taken in most models to describe sliding friction, which essentially pose an identical problem as that faced in understanding tribochemistry, that of calculating how an external force increases the rate of the transition from one stable or metastable state to another over an activation barrier [39]. In the case of sliding friction, the initial and final states are identical and only energy is dissipated, while in tribochemical reactions (and nanoscale wear) the initial (reactant) and final (product) states differ. The first section will therefore discuss models in which the forces lie within the reaction coordinate plane and will lead to the most commonly used Bell model [40] and its variants [41].

The next section of this paper will discuss more general models that do not insist that the forces be aligned within the plane of the reaction coordinate and explores the influence that this could have on the tribochemical properties. The following section briefly explores the ways in which changes in the contact, for example the interpenetration of adsorbates, can affect the tribochemical reactivity, and the last section will analyse currently available experimental results considering the above discussions.

3 One-Dimensional Tribochemical Models with Forces Aligned Along the Plane of the Reaction Coordinate

3.1 A Rigid-Potential Model: The Bell Equation

The simplest model for calculating the rate constant $k(\underline{F})$ under the influence of a shear force vector $\underline{F}$ is the Bell model [40], which has also been called the Bell–Evans (B–E) or the Bell–Evans–Zhurkov models. This model imagines a reactant state at $x = 0$, with the transition state located a distance $\Delta\underline{x}^{\ddagger}$ from it along the reaction coordinate defined as the x axis. $\Delta x^{\ddagger}$, the magnitude of $\Delta\underline{x}^{\ddagger}$, is referred to as the activation length. The B–E model assumes that the shape of the potential energy curve from the reactant to the transition state to the product is not influenced by the external force. Consequently, the work carried out on the system lowers the height of the activation barrier E_{act} by an amount $\underline{F} \cdot \Delta\underline{x}^{\ddagger}$. If F is the magnitude of the component of the force along x, this yields an effective activation energy under the influence of the applied force of $E_{\text{act}} - F\Delta x^{\ddagger}$. If

the force F is aligned within the plane of the reaction coordinate, then $\underline{F} \cdot \Delta\underline{x}^{\ddagger} = F\Delta x^{\ddagger}$. It is also assumed that the pre-exponential factor A is not unduly influenced by the external force, so that the rate constant for the rate of the forward reaction from an initial state at $x = 0$ is:

$$k(F) = A \exp\left(-\frac{E_{\text{act}} - F\Delta x^{\ddagger}}{k_{\text{B}}T}\right). \quad (1)$$

Note that the rate of the reverse reaction, from the product to the initial reactant state, is also influenced by the external force. Here, however, the effect of the external force is to increase this barrier. Thus, the combination of the forward and reverse rates is proportional to $\sinh\left(\frac{F\Delta x^{\ddagger}}{k_{\text{B}}T}\right)$, and this equation has been used by Eyring to model viscosity [39, 42, 43]. In the following, it is assumed that the product of the shear-induced reaction is much more stable than the reactant, so that the rate of the reverse reaction is negligible. The thermal rate constant k_0 for the reaction is given by $A \exp\left(-\frac{E_{\text{act}}}{k_{\text{B}}T}\right)$, so that the B–E equation becomes:

$$k(F) = k_0 \exp\left(\frac{F\Delta x^{\ddagger}}{k_{\text{B}}T}\right). \quad (2)$$

This predicts an exponential increase in the reaction rate with applied force as found experimentally [23, 24]. It is more usual to measure the influence of shear stress on reaction rate, $k(\sigma)$ where $\sigma = F/A_{\text{r}}$, and A_{r} is the area of the reactant on which the shear stress acts. In this case, the B–E equation becomes:

$$k(\sigma) = k_0 \exp\left(\frac{\sigma A_{\text{r}}\Delta x^{\ddagger}}{k_{\text{B}}T}\right) = k_0 \exp\left(\frac{\sigma\Delta V^{\ddagger}}{k_{\text{B}}T}\right), \quad (3)$$

where $\Delta V^{\ddagger}$ is often referred to as the activation volume, originally coined for solution-phase reactions [44] and dislocation motion [45–49]. The value of A_{r} is often difficult to determine precisely since it depends in detail on the contact conditions, the number of reactant molecules on the surface and the way in which the force is exerted.

3.2 Second-Order Effects: The Influence of Shape of the Energy Profile on Reaction Kinetics

Unlike transition-state theory, in which the reaction rate depends primarily on the height of the activation barrier, an external force can influence the shape of the reaction potential to give second-order (F^2) effects. This can be illustrated by expanding the initial- and transition-state energy profiles to second order in position, thus modelling them by parabolas in a similar way as used by Evans and Polanyi [44] and in Marcus theory [50]. This perturbation approach is only applicable to relative low applied forces, but it does allow some general insights into the effect of potential shape on tribochemical reactions to be obtained and is known as the extended-Bell model [41].

In the following, energies are referenced to the initial (reactant) state, taken to be at the origin of the reaction coordinate, $x = 0$. The initial-state potential can be expanded to second order in x as $V_{\text{I}}(x) = \frac{x^2}{2\chi_{\text{I}}}$, where χ_{I} is the (positive) curvature of the initial-state potential along the reaction coordinate; $\chi_{\text{I}} = \frac{1}{\left.\frac{\partial^2 V(x)}{\partial x^2}\right|_0}$, and is the inverse of the force constant. A similar Taylor series expansion is carried out for the transition state. As noted above, the transition state is a local maximum along the reaction coordinate, although, in general, it is a saddle point. This yields $V_{\text{T}}(x) = E_{\text{act}} + \frac{\left(x-\Delta x^{\ddagger}\right)^2}{2\chi_{\text{T}}}$ for the transition state, where χ_{T} is the value of the (negative) curvature at the transition state, given by $\chi_{\text{T}} = \frac{1}{\left.\frac{\partial^2 V(x)}{\partial x^2}\right|_{\Delta x^{\ddagger}}}$ [41]. As above, the effect of an imposed force F is calculated from the turning points of the initial- and transition-state potentials by adding a potential due to a force along the direction of the reaction coordinate; $-Fx$. The initial-state local potential energy profile becomes $V_{\text{I}}(x, F) = \frac{x^2}{2\chi_{\text{I}}} - Fx$ and reveals that the initial-state minimum shifts with force to a higher value along the reaction coordinate to give $x_{\min} = +F\chi_{\text{I}}$. Similarly, because of the negative curvature of the transition state, the effect of an external force is to move it to lower values of the reaction coordinate. $x_{\max} = \Delta x^{\ddagger} + F\chi_{\text{T}}$; the external force modifies the shape of the potential in addition to lowering the barrier. Since the initial and transition states along the reaction coordinate have positive and negative curvatures, respectively, in such a one-dimensional model, the initial and transition states will always move towards each other under the influence of an external force. However, since the transition state is, in general, a saddle point, the direction of the force relative to the reaction coordinate can change the way in which the position of the transition state moves; these effects will be discussed in Sect. 4.

The resulting activation barrier under the influence of the external force is now given by:

$$E_{\text{act}}(F) = E_{\text{act}} - F\Delta x^{\ddagger} + \frac{F^2}{2}(\chi_{\text{I}} - \chi_{\text{T}}). \quad (4)$$

The first two-terms are identical to those for a rigid potential (the B–E model, Eq. 1), while the second-order terms are due to a modification of the shape of the potential

under the influence of an external force. This can again be written in terms of the shear stress as:

$$E_{\mathrm{act}}(\sigma) = E_{\mathrm{act}} - \sigma A_{\mathrm{r}} \Delta x^{\ddagger} + \frac{\sigma^2 A_{\mathrm{r}}^2}{2}(\chi_{\mathrm{I}} - \chi_{\mathrm{T}}). \quad (5)$$

Thus, a quadratic term is expected in the shear-stress dependence of the activation energy $E_{\mathrm{act}}(\sigma)$, and hence on $\ln(k(\sigma))$. This results in the value of the activation length decreasing with increase shear stress, so that the second-order term is always positive, as in Eq. 5 because the initial and transition state move closer to each other as the shear stress increases. This is referred to as the Hammond effect [51, 52].

In addition, as noted above, such a Taylor series expansion only allows the effect of relatively low forces to be explored because it only describes the shape of the energy profile near the turning points. This can be addressed by selecting a continuous function of x that has an initial minimum and a transition state with adjustable curvatures and is discussed in the next section.

3.3 More Complete Analysis of the Influence of Shape of the Energy Profile on Reaction Kinetics

An alternative approach is to use a continuous function of x which allows the curvatures of the initial and transition states to be varied in a systematic way, for example, using the Remoissenet–Peyrard (R–P) potential [53]:

$$V(x,r) = \frac{E_{\mathrm{act}}(1-r)^2}{2} \times \frac{1 - \cos\left(\frac{\pi x}{\Delta x^{\ddagger}}\right)}{\left(1 + r^2 + 2r\cos\left(\frac{\pi x}{\Delta x^{\ddagger}}\right)\right)}, \quad (6)$$

where E_{act} is the barrier height, $\Delta x^{\ddagger}$ is the position of its maximum and $|r|<1$. Positive values of r yield a sharp transition state and negative values a sharp initial state, where the initial- and transition-state curvatures depend on the value of r and are given by:

$$\chi_{\mathrm{I}} = \frac{2\Delta x^{\ddagger 2}}{E_{\mathrm{act}}\pi^2}\left(\frac{1+r}{1-r}\right)^2 \text{ and } \chi_T = -\frac{2\Delta x^{\ddagger 2}}{E_{\mathrm{act}}\pi^2}\left(\frac{1-r}{1+r}\right)^2. \quad (7)$$

The influence of an external force is described by subtracting Fx from the right-hand side of Eq. (6) to give:

$$V(x,r,F) = \frac{E_{\mathrm{act}}(1-r)^2}{2} \times \frac{1 - \cos\left(\frac{\pi x}{\Delta x^{\ddagger}}\right)}{\left(1 + r^2 + 2r\cos\left(\frac{\pi x}{\Delta x^{\ddagger}}\right)\right)} - Fx \quad (8)$$

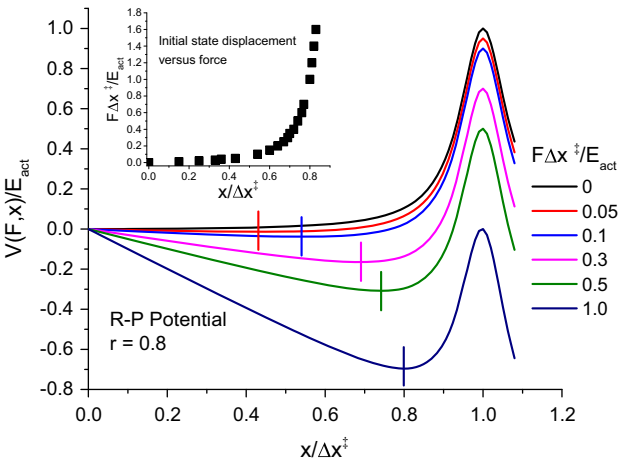

Fig. 1 Shape of the R–P potential for $r = 0.8$, at different forces F. Shown as an *inset* is the change in the position of the initial minimum with F

This equation is shown plotted in Fig. 1 for various values of F, where the activation barrier E_{act} and $\Delta x^{\ddagger}$ are normalized to unity, for a relatively high value of $r = 0.8$. The position of the sharp transition state only changes very slightly with a change in F in accord with the extended-Bell model described above (Sect. 3.2), while the minimum of the much shallower initial state moves rapidly with increasing values of F from $x = 0$ to close to the position of the transition state (see inset to Fig. 1).

3.3.1 *Approximate Solutions for the Force-Dependent Energy Barrier for the R–P Potential*

Equations of the type shown in Eq. 8 are not generally analytically soluble even for simple sinusoidal potentials [39, 54, 55]. However, the general behaviour is that the activation barrier $E_{\mathrm{act}}(F)$ decreases from an initial value of E_{act} as the force increases. Approximate solutions can be obtained for two regimes [54]. First, solutions can be found for low forces by carrying out Taylor series expansions of the potential around the maximum and minimum. Second, Prandtl also showed that $E_{\mathrm{act}}(F)$ tends to zero at a sufficiently high force, generally designated, F^*, and that the activation barrier asymptotically approaches zero as $(F^* - F)^{3/2}$ [39, 54]. Note that this function can be also fit to a quadratic equation and is therefore mathematically equivalent to the extended-Bell model. Both approaches are illustrated in the following for the R–P potential (Eq. 8).

The value of F^* is first calculated for the R–P potential. The first derivative of the modified R–P potential (Eq. 8) is given by:

$$\frac{1}{E_{\mathrm{act}}}\frac{\partial V}{\partial x}\bigg|_{\mathrm{r,F}} = \frac{(1-r)^2}{2} \times \frac{\pi(1+r)^2 \sin\left(\frac{\pi x}{\Delta x^{\ddagger}}\right)}{\Delta x^{\ddagger}\left(2r\cos\left(\frac{\pi x}{\Delta x^{\ddagger}}\right)+(1+r^2)\right)^2} - \frac{F}{E_{\mathrm{act}}} = 0, \tag{9}$$

which is set to zero to define the turning points at a force F. The force reaches the critical value of F^* at a distance x^* when the second derivative of the potential equals zero:

$$\frac{1}{E_{\mathrm{act}}}\frac{\partial^2 V}{\partial x^2}\bigg|_{r,F} = \frac{(1-r)^2}{2} \times \frac{\pi^2(1+r)^2\left(4r\sin^2\left(\frac{\pi x^*}{\Delta x^{\ddagger}}\right)+2r\cos^2\left(\frac{\pi x^*}{\Delta x^{\ddagger}}\right)+(1+r^2)\cos\left(\frac{\pi x^*}{\Delta x^{\ddagger}}\right)\right)}{\Delta x^{\ddagger 2}\left(2r\cos\left(\frac{\pi x^*}{\Delta x^{\ddagger}}\right)+(1+r^2)\right)^3} = 0. \tag{10}$$

The solution is given by

$$4r\sin^2\left(\frac{\pi x^*}{\Delta x^{\ddagger}}\right)+2r\cos^2\left(\frac{\pi x^*}{\Delta x^{\ddagger}}\right)+(1+r^2)\cos\left(\frac{\pi x^*}{\Delta x^{\ddagger}}\right)=0$$

. Substituting for $\sin^2$ gives a quadratic equation in $\cos\left(\frac{\pi x^*}{\Delta x^{\ddagger}}\right)$ as:

$$2r\cos^2\left(\frac{\pi x^*}{\Delta x^{\ddagger}}\right)-(1+r^2)\cos\left(\frac{\pi x^*}{\Delta x^{\ddagger}}\right)+4r=0. \tag{11}$$

This can easily be solved to yield:

$$\cos\left(\frac{\pi x^*}{\Delta x^{\ddagger}}\right) = \frac{(1+r^2)-\sqrt{(1+r^2)^2+32r^2}}{4r}, \tag{12}$$

and $\sin\left(\frac{\pi x^*}{\Delta x^{\ddagger}}\right) = \sqrt{1-\cos^2\left(\frac{\pi x^*}{\Delta x^{\ddagger}}\right)}$. The resulting value of F^* is obtained by substitution into:

$$\frac{F^*}{E_{\mathrm{act}}} = \frac{(1-r)^2}{2} \times \frac{\pi(1+r)^2\sin\left(\frac{\pi x^*}{\Delta x^{\ddagger}}\right)}{\Delta x^{\ddagger}\left(2r\cos\left(\frac{\pi x^*}{\Delta x^{\ddagger}}\right)+(1+r^2)\right)^2}, \tag{13}$$

from Eq. 9. Now, from Eq. 12, $\cos\left(\frac{\pi x^*}{\Delta x^{\ddagger}},+r\right) = -\cos\left(\frac{\pi x^*}{\Delta x^{\ddagger}},-r\right)$ and $\sin\left(\frac{\pi x^*}{\Delta x^{\ddagger}},+r\right) = \sin\left(\frac{\pi x^*}{\Delta x^{\ddagger}},-r\right)$. Substituting into Eq. 13 shows that $\frac{F^*\Delta x^{\ddagger}}{E_{\mathrm{act}}}$ is the same for positive and negative values of r, so that the solution is identical irrespective of whether the initial or the transition-state potential is sharp.

In order to confirm this result, the value of F^* was obtained numerically by increasing the value of F until the barrier had decreased to zero. As shown in Fig. 2, the numerical and analytical solutions are in excellent agreement. These results also emphasize that the shape of the potential has a strong influence on tribochemical reactions.

We now obtain the solution at low values of F. This is obtained by carrying out Taylor series expansions of Eq. 9 to second order in F about $\frac{x}{\Delta x^{\ddagger}} = 0$ for the minimum and $\frac{x}{\Delta x^{\ddagger}} = 1$ for the maximum to obtain equations for $x_{\min}(F)$ and $x_{\max}(F)$. The resulting values are then substituted into Eq. 8 to obtain the corresponding energies at the minimum and maximum, $E_{\min}(r,F)$ and $E_{\max}(r,F)$ as a function of F to yield the height of the barrier $E_{\mathrm{act}}(F) = E_{\max}(r,F) - E_{\min}(r,F)$ to second order to yield:

$$E_{\mathrm{act}}(F) = E_{\mathrm{act}} - F\Delta x^{\ddagger} + \frac{\left(F\Delta x^{\ddagger}\right)^2}{E_{\mathrm{act}}\pi^2}\left(\left(\frac{1+r}{1-r}\right)^2+\left(\frac{1-r}{1+r}\right)^2\right). \tag{14}$$

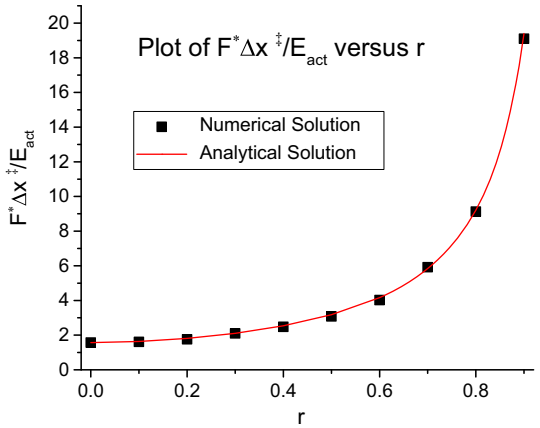

Fig. 2 Plot of the numerical solution of $F\Delta x^{\ddagger}/E_0$ versus r (*filled square*) for a R–P potential compared with the analytical solution from Eq. 13 (*red line*) (Color figure online)

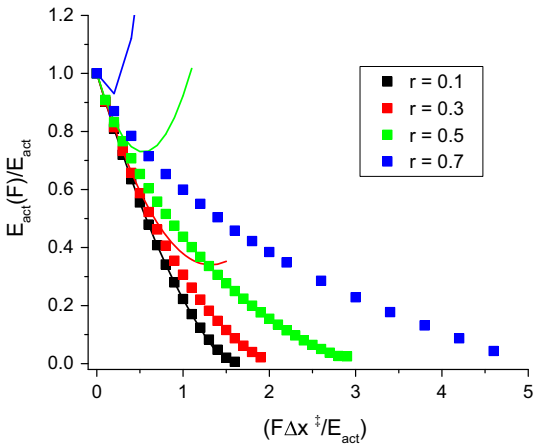

Fig. 3 Plot of the numerically determined activation barrier for an R–P potential under the influence of a force, F, $E_{act}(F)$ normalized to the height of the barrier in the absence of an external force (E_{act}) as a function of the normalized external force, $F\Delta x^{\ddagger}/E_{act}$, for $r = 0.1$ (*black square*), $r = 0.3$ (*red square*), $r = 0.4$ (*green square*), and $r = 0.7$ (*blue square*). The *solid lines* show the results of a second-order expansion in F, corresponding to the extended-Bell model (Color figure online)

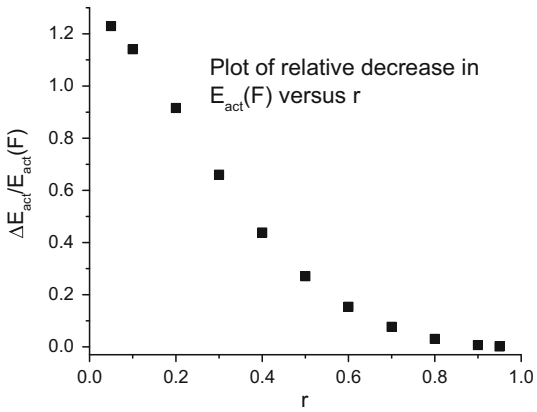

Fig. 4 Plot of the maximum relative decrease in force-induced activation barrier as a function of r for a second-order expansion of the R–P potential

There are several points to note about this result. First, as found for F^*, the variation in activation energy with force is symmetrical in r; that is $E_{act}(F, +r) = E_{act}(F, -r)$ so that the behaviour is identical for a sharp initial state and shallow transition state, and vice versa. Second, this formula is exactly that which would have been obtained from the extended-Bell model (Eq. 4) by substituting the curvature for the initial and final states (Eq. 7). Finally, the Taylor series expansion of $E_{act}(F)$ to only second order means that the activation energy decreases with increasing F, but the reaches a minimum, and then starts to increase again. This is illustrated in Fig. 3 where numerical measurements of $E_{act}(F)/E_{act}$ are shown plotted versus $\left(\frac{F\Delta x^{\ddagger}}{E_{act}}\right)$ for different values of r (as solid squares). The solid lines in the corresponding color show the variation predicted by Eq. 14. This reveals that the initial decrease in activation barrier at low forces is relatively well reproduced for low values of r ($r = 0.1$ (black square), $r = 0.3$ (red square)), less well for $r = 0.5$ (green square), but not at all well reproduced for $r = 0.7$ (dark blue square). This is further illustrated in Fig. 4 which plots the relative energy decrease $\Delta E_{act}(F)/E_{act}$ at the minimum in the extended-Bell model (Eq. 14) as a function of r. Significant decreases in energy barrier are reproduced only for low values of r. This is a direct consequence of the shape of the potential. In the case of a sharp transition state and shallow initial state, the position of the energy minimum rapidly increases giving an initial, somewhat nonlinear dependence of energy barrier on F. As this minimum moves closer to the transition state, it changes position only slowly resulting in a relatively constant value of the energy minimum at some value $\alpha(r)\Delta x^{\ddagger}$, where α becomes close to unity. The energy minimum decreases as $-\alpha\Delta x^{\ddagger}F$, while the energy maximum decreases as $-\Delta x^{\ddagger}F$ to produce a relatively slow variation in the height of the activation barrier with force, resulting in large F^* values for large values of r in the R–P potential (Fig. 2). This indicates that while the solution obtained by a Taylor series expansion of the potential yields a good approximation to the correct solution for small values of r (when the potential is close to sinusoidal in shape), it is a worse approximation at higher r values. This is addressed in the next section by obtaining numerical solutions to Eq. 8.

3.3.2 *Numerical Solutions for the Force-Dependent Energy Barrier for the R–P Potential*

Based on the above discussion, the general form of the change in energy barrier as a function of F can to a good approximation be written as:

$$E_{act}(F) = E_{act} - \alpha(r)F\Delta x^{\ddagger} + \beta(r)\frac{\left(F\Delta x^{\ddagger}\right)^2}{E_{act}}. \qquad (15)$$

The values of $\alpha(r)$ and $\beta(r)$ are determined by numerically solving Eq. 8. It is found that fits to Eq. 15 become less good as $E_{act}(F)$ approaches zero, particularly for larger values of r. Consequently, numerical fits are carried out for barrier height reductions of $\leq$40% since this is the range of barrier reductions most likely to be found in experiment (see Sect. 7), and results in better fits to Eq. 15. The resulting fits are displayed in Fig. 5. They show that quadratic fits are reasonable for $r \leq 0.7$, but fail to accurately capture the initial nonlinear decrease at low forces and the subsequent approximately linear behaviour at high forces, for larger

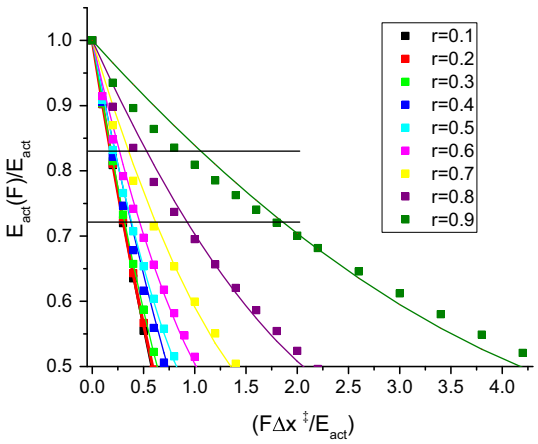

Fig. 5 Plot of the numerically determined activation barriers under the influence of a force, F, $E_{act}(F)$ normalized to the height of the barrier in the absence of an external force (E_{act}) as a function of the normalized external force, $F\Delta x^{\ddagger}/E_{act}$, for $r = 0.1$ (*black square*), $r = 0.2$ (*red square*), $r = 0.3$ (*green square*), $r = 0.4$ (*dark blue square*), $r = 0.5$ (*light blue square*), $r = 0.6$ (*violet square*), $r = 0.7$ (*yellow square*), $r = 0.8$ (*red square*) and $r = 0.9$ (*green square*). The *solid lines* show the results of a quadratic fit to the data. The *horizontal lines* indicate the energy range for which the tribochemical ZDDP film formation rates were measured [21] (Color figure online)

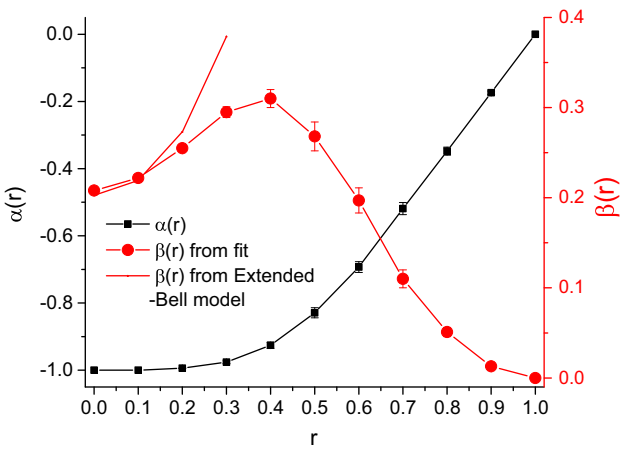

Fig. 6 Plot of the coefficients of the linear ($\alpha(r)$) and quadratic ($\beta(r)$) terms derived from a fit to the numerical solutions to the R–P potentials shown in Fig. 5, displayed as a function of r. Shown also as a solid line are the calculated values of $\beta(r)$ from the extended-Bell model

values of r. The results also emphasize the influence of potential shape on tribochemical reactivity, where larger values of r require an amount of external work to be carried out on the system that is greater than the overall activation barrier for the thermal reaction. This is in accord with the results shown in Fig. 2, where the value of F^* increases with increasing values of r. These results indicate that the shape of the potential energy curve strongly influences the tribochemical stability of the reactant. For example, the simple Bell model predicts that the stress-induced barrier should decrease to zero at $F^* = \Delta x^{\ddagger}/E_{act}$. In general, the Hammond effect requires larger forces to reduce the activation barrier by some amount, and this effect becomes more pronounced as the value of r increases, implying that a reactant with a sharp initial or transition state will be more stable under shear than one with more similar curvatures in the initial and transitions states, for the same barrier heights and activation lengths.

The use of this equation to analyse the existing tribochemical experiments will be discussed in greater detail in Sect. 7. The resulting values of $\alpha(r)$ and $\beta(r)$ are shown plotted as a function of r in Fig. 6. The value of α deviates from the value of -1 expected for the Bell and extended-Bell models, decreasing to zero as the value of r approaches unity. Similarly, the value of β is reasonably close to the prediction of the extended-Bell model only for r values ≤ 0.2, reaches a maximum at $r \sim 0.4$, and then decreases asymptotically to zero as r tends to unity. It should be noted that the values of α and β become less precise at higher r values because the quadratic fits are less good for these potentials (Fig. 5). Finally, as noted above, identical results are obtained for positive and negative values of r, that is $E_{act}(F, +r) = E_{act}(F, -r)$.

In summary, at low forces, the main effect is to lower the transition-state energy by an amount $F \times \Delta x^{\ddagger}$, as in the B–E model. However, the external force also shifts the positions of both the initial and transition states, thereby leading to deviations from the B–E model as discussed in Sect. 3.2. The barrier $E_{act}(F, r)$ can be obtained numerically from plots such as those shown in Figs. 5 and 6. The results deviate from the rigid-potential B–E equation and also have an F^2 dependence. For relatively low values of r (<0.2), the results are quite well reproduced by carrying out a Taylor series expansion of the R–P about the energy maxima and minima (Eq. 14). However, the sharper potentials cause this approximation to be less valid for higher r values.

4 Influence of the Direction of the Applied Force on Tribochemistry

In the preceding sections, the effect of an external shear force was analysed by considering forces that lie within the plane of the reaction coordinate, which describes the lowest-energy pathway from the initial, reactant state to the final product. However, different behaviour can occur when the forces are not collinear with the reaction coordinate plane, including the so-called anti-Hammond and catch-bond behavior, and this has recently been nicely illustrated using a model potential energy surface [38]. No such effects have yet been observed in tribochemical reactions, although there is some evidence for the existence

of the Hammond effect (see Sect. 7). Whether such effects do occur will depend on how rigidly the adsorbates are bound to the surface, for example, whether they can rotate azimuthally under the influence of a force. Furthermore, many molecules will be present within the contact, even in nanoscale AFM experiments, which will result in a range of orientations of the shear force with respect to the reaction coordinate. Understanding such effects will require a detailed knowledge of the structure of the reactant.

In the situation analysed in the previous sections, when the applied shear force is collinear with the reaction coordinate, the curvature of the transition state is always negative thus causing the position of the transition state to move towards the initial (reactant) state, while the reactant state always moves towards the transition state, giving rise to a positive second-order terms (see Sects. 3.2, 3.3), known as the Hammond effect. However, the potential energy surface around the transition state forms a saddle point so that, for example, in the case of a force applied with a significant component perpendicular to the reaction coordinate, the curvature of the transition state will be positive, causing a second-order effect in which the transition state moves away from the initial state (hence the nomenclature anti-Hammond effect [56]). If the transition-state curvature is such that it moves more rapidly with force than the initial state, this can result in negative values of β in Eq. 15.

An unusual effect can also arise in which the reaction rate can initially decrease and then increase with force. This essentially arises when the applied force has a large component in a direction opposite to the vector between the initial and transition states, resulting in an initial increase in the energy barrier, eventually decreasing at higher forces, in a behaviour known as a catch-bond [57, 58].

It is not clear as to the extent such mechanisms apply to the shear-induced tribochemistry of adsorbates on surfaces since the amount of experimental data to date on such systems is sparse. The results that are discussed in Sect. 7 appear to show either Bell-like behaviour or evidence for the Hammond effect. However, as recently pointed out, [38] such effects are often difficult to establish experimentally. In particular, the curvatures of plots of ln(rate) or activation barrier versus shear stress are difficult to discern within the experimental error.

5 Effect of Contact Pressure

5.1 Background

The above analyses explore the influence of shear forces on increasing tribochemical reaction rates. However, shear stresses invariably occur under the influence of a normal load. For example, it has been found that the height of the sliding potential in the Prandtl-Tomlinson model [55, 59] changes with applied load. It was inherently assumed in the tribochemical models discussed above that the motion from the initial to the transition state is exclusively parallel to the shear stress. It is, however, likely that the trajectory is accompanied by a vertical motion. In this case, the work carried out on the system becomes $F_{\mathrm{L}} \times x + F_{\mathrm{N}} \times z$, where F_{L} and F_{N} are the lateral and normal forces where the ratio $\frac{F_{\mathrm{L}}}{F_{\mathrm{N}}} = \mu$ (the friction coefficient). Thus, the reaction coordinate will, in general, include both lateral and vertical motions as the reaction proceeds from the initial to the transition state so that, in the context of a model in which these forces lie within the plane of the reaction coordinate, the potential is given by $V = V(x, z)$. However, the variation in z coordinate depends on the values of x; $z = z(x)$, so that $V = V(x, z(x))$. In this case, the combined potential is written as:

$$V(x, F) = V(x, z(x)) - F\left(x + \frac{z(x)}{\mu}\right). \tag{16}$$

Thus, within the simple Bell model formalism that neglects the effects of potential shape on the activation barrier (see Eq. 2), this gives:

$$k(F) = k_0 \exp\left(\frac{F\left(\Delta x^{\ddagger} + \frac{z\left(\Delta x^{\ddagger}\right)}{\mu}\right)}{k_{\mathrm{B}}T}\right) = k_0 \exp\left(\frac{F\Delta x_{\mathrm{eff}}^{\ddagger}}{k_{\mathrm{B}}T}\right), \tag{17}$$

where $\Delta x_{\mathrm{eff}}^{\ddagger}$ is an effective activation length. This will produce larger effects than just considering the lateral motion alone, but requires a detailed knowledge of the reaction pathway to allow the relationship between the lateral and vertical motions to be described. However, while the tribochemical reaction pathways have, in most cases, not yet been clearly defined, the relatively few tribochemical systems studied to this point appear to involve molecular decomposition. For example, the shear-induced reaction of alkyl thiolate species involves the adsorbate tilting (so includes both lateral and vertical motion), resulting in C–S bond scission [25]. Similarly, the tribochemistry of oxygenated graphene involves carbon–oxygen bond scission [24], while it is likely that the formation of anti-wear films from ZDDP is initiated by removal of the alkyl groups. Consequently, a simple model is developed in the next section to illustrate such shear- and pressure-induced effects for molecular decomposition.

5.2 Shear and Normal Stress Effects on Decomposition of a Rigid Molecular System

We will use a simple model in which a rigid adsorbate of length d is initially oriented at some polar angle θ_0 and an azimuthal angle φ_0 with respect to the surface normal. It is supposed that an increase in the tilt angle θ towards the surface leads to some reaction where the lateral distance of the molecule from the initial to the transition state is $\Delta x^{\ddagger}$. In this case, a lateral motion of the molecular terminus by an amount Δx is accompanied by a motion by a distance Δz towards the surface. In addition, an adsorbed molecule may be able to rotate relatively freely azimuthally about a normal to the surface (taken to be the z direction), so that a shear force is likely to initially orient the molecule such that the force is directed from the initial towards the transition state, thus warranting the use of a one-dimensional model in this case. Hindered rotation will give more complex behaviour, which will depend on the height of the barrier to azimuthal rotation compared to the activation barrier and the orientation of the molecule with respect to the shear force, which might produce effects such as those described in Sect. 4.

As indicated in Sect. 5.1, the analysis requires that Δz be obtained as a function of Δx, and this will be done by assuming that the molecule behaves as a rigid rod. If the initial x coordinate of the molecular terminus is x_0, which moves to a position x in the reaction coordinate plane when a force is applied, then $x_0^2 + z_0^2 = x^2 + z^2 = d^2$. The molecular terminus then moves downwards (in the negative z direction) by an amount $\Delta z = z_0 - z$ and laterally by $\Delta x = x - x_0$. A straightforward manipulation of these equations gives:

$$\Delta z = \tan\theta_0 \Delta x \tag{18}$$

in the limit of $\Delta x \ll d$. Substituting into Eq. 17 gives:

$$k(F) = k_0 \exp\left(\frac{F\Delta x^{\ddagger}}{k_B T}\left(1 + \frac{\tan\theta_0}{\mu}\right)\right), \tag{19}$$

so that $\Delta x_{\text{eff}}^{\ddagger} = \Delta x^{\ddagger}\left(1 + \frac{\tan\Theta_0}{\mu}\right)$. This indicates that an initially tilted molecule will have a larger effective value of $\Delta x^{\ddagger}$ due to the additional work done on the system by the normal force.

6 Effect of Sliding Velocity: Force Distributions Within Contact

Up to this point, there have been no experiments to study the effect of the way in which the force is coupled into the tribochemical reaction and the resulting effect of sliding velocity on the rates. The atom in the contact that exerts the force to induce the chemical reaction has been referred to as a "pilot atom" [60]. Nevertheless, it is worth exploring how sliding speed might influence the rates of tribochemical reactions. Within a simple Prandtl-Tomlinson framework, the friction force depends on the sliding velocity. This can be analysed in a straightforward way for constant-force sliding with a sinusoidal potential of height E_S and periodicity a [39], which is found to depend on the force as:

$$E_S(F) = E_S - \frac{Fa}{2} + \frac{E_S}{2}\left(\frac{F}{F^*}\right)^2, \tag{20}$$

for $F \ll F^*$, where $F^* = \frac{\pi E_0}{a}$. Note that the form of this equation is analogous to that for the extended-Bell model (Eq. 4) since similar concepts are used to derive both. Ignoring second-order terms for simplicity gives:

$$E_S(F) \cong E_S - \frac{Fa}{2}. \tag{21}$$

Here, the value of E_S is different from the reaction activation energy E_{act}, where the former value describes the interaction between the contacting molecules on the surface and the way in which the force is exerted.

However, it may be that the adsorbed molecules at the contacting interface can also interpenetrate giving rise to a time-dependent evolution of the energy barrier for sliding. Such changes in the contact are generally described using rate-state theory, which postulates a time-dependent change in the state of the system that influences effects such as stick–slip behaviour. This is modelled in the following by assuming that the contact evolves over time such that the sliding barrier is E_S and slowly varies such that $E_S(t) = E_S + \Delta E_S(t)$, where $\Delta E_S(t)$ is a single-valued, monotonically increasing function of t, where $\Delta E_S(t = 0) = 0$. In this case:

$$E_S(F, t) = E_S + \Delta E_S(t) - \frac{Fa}{2}. \tag{22}$$

Following Eyring [39, 42], it is argued that the value of the constant force F adjusts to yield an average time to transit the energy barrier equal to $\frac{a}{v}$, where v is the sliding velocity, to give:

$$v = aP \exp\left(-\frac{E_S(F, t)}{k_B T}\right), \tag{23}$$

where P is a pre-exponential factor for transition over the barrier (analogous to the reaction pre-exponential factor A (Eq. 1)). The values for a reaction and sliding over a barrier may be quite different. This gives:

$$E_S(F, t) = k_B T \ln\left(\frac{aP}{v}\right). \tag{24}$$

The time for the contact to evolve during sliding is $\sim \frac{a}{v}$ so that equating Eqs. (22) and (24) gives:

$$E_S + \Delta E_S\left(\frac{a}{v}\right) - \frac{Fa}{2} = k_B T \ln\left(\frac{aP}{v}\right), \tag{25}$$

to yield: $F = \frac{2F^*}{\pi} + \frac{2k_B T}{a}\ln\left(\frac{v}{aP}\right) + \frac{2}{a}\Delta E_S\left(\frac{a}{v}\right)$. The form of $\Delta E_S(t)$ will depend on the kinetic process at the interface that leads to an increase in barrier and could be due to the plastic deformation of asperities, the slow formation of chemical bonds (i.e. Carpick [61]), or an adjustment of the interfacial structure. A suitable function that has the required properties is $\Delta E_a(t) \sim \Delta E \ln\left(1 + \frac{t}{t_c}\right)$ where t_c is some characteristic time. This gives:

$$F = \frac{2F^*}{\pi} + \frac{2k_B T}{a}\ln\left(\frac{v}{aP}\right) + \frac{2}{a}\Delta E \ln\left(1 + \frac{a}{t_c v}\right), \tag{26}$$

which is identical to the steady-state solution of the rate-state formalism. In the case of a simple Bell model (Eq. 2), this yields:

$$\ln k(v) = \ln k_0 + \frac{\Delta x^{\ddagger}}{k_B T}\left(\left(\frac{2F^*}{\pi}\right) + \frac{2k_B T}{a}\ln\left(\frac{v}{aP}\right) - \frac{2}{a}\Delta E \ln\left(\frac{t_c v}{a}\right)\right), \tag{27}$$

assuming that $\frac{a}{t_c v} \gg 1$. Consequently, this suggests that $\ln k$ (or E_a) depends logarithmically on the sliding velocity, but can either increase or decrease depending on the value of ΔE compared to $k_B T$ and suggests an alternative strategy for probing shear-induced tribochemical reactions.

However, a wide range of local contacts are likely to occur between the interacting molecules at the interface to give a distribution of forces [25]. In the case of calculations of the friction force (Eq. 27), the parameters will reflect some average of all contacts. However, in tribochemical reactions, the highest forces will have a larger influence on the reaction rates than the lower ones so that, in such cases, it may also be necessary to know what the force distribution is to correctly model the behaviour [25].

7 Analysis of Experimental Tribochemical Kinetics

7.1 Summary of Results

The above analyses reveal the potential complexities of shear-induced reactions on surfaces and that a molecular-level description of these phenomena will require understanding the structure and dynamical properties of the reactant. One of the central issues in relating the influence of a shear force on enhancing surface chemical reaction rates is to define the forces that act on an individual molecule. This will depend on the number of molecules in the contact and the way in which the force is exerted on each molecule, and whether there is a distribution of forces [25, 62]. An additional key issue is the way in which the external force is aligned with respect to the reactive potential energy surface and, in particular, whether it is collinear with the lowest energy pathway, that is, in the plane of the reaction coordinate. This is turn will depend on whether the reactant or a particular portion of the reactant can reorient so that the plane of the reaction coordinate contains the shear direction. In such cases, perhaps the most promising avenue is to explore molecules that mimic the rigid adsorbates anchored to the surface at one end (as discussed in Sect. 5.2), that can azimuthally rotate so that the adsorbate initially aligns with the shear direction, so that load and shear combine to induce molecular tilt towards a reaction transition state. Adsorbates that are not able to reorient in this way may well show the unusual effects (discussed in Sect. 4).

Finally, sliding-induced (both shear and load) reaction rate constants depend on the shape of the energy profile. This requires much more information on the details of the reaction energy profile than do thermally induced reactions that depend primarily on the height of the energy barrier (the activation energy).

Nevertheless, it is worth discussing the way in which currently available experimental data can be analysed to provide information on the nature of the reaction energy profile, the height of the energy barrier, and some information on an effective activation length. In general, any tribochemical kinetic data will consist of a measurement of an effective reaction rate constant as a function of either normal load, lateral force or, under ideal circumstances, a shear stress. In the case of experiments where rates are measured as a function of lateral force, the above analyses (Eq. 15) indicate that the activation barrier $E_{act}(F)$ depends quadratically on F:

$$E_{act}(F) = E_{act} - \alpha(r) F \Delta x^{\ddagger}_{eff} + \beta(r)\frac{\left(F\Delta x^{\ddagger}_{eff}\right)^2}{E_{act}}. \tag{28}$$

where $\Delta x^{\ddagger}_{eff}$ is used to indicate that the evolution from the initial to the transition state can involve both vertical and lateral motions in the plane (see Sect. 5) and may depend on velocity (see Sect. 6).

Since the force acting on each adsorbate is not known, it will, for simplicity, be assumed that the forces are uniformly distributed over the contact. In addition, the reaction rate is either generally measured as a function of the shear stress σ or the contact pressure P, where $\frac{\sigma}{P} = \mu$, the friction coefficient. Following the discussion in Sect. 3.1,

we write $F = \sigma A_r$, where A_r is the area on the surface occupied by each reactant. Now Eq. 28 becomes:

$$E_{act}(\sigma) = E_{act} + \alpha(r)\sigma\Delta V_{eff}^{\ddagger} + \beta(r)\frac{\left(\sigma\Delta V_{eff}^{\ddagger}\right)^2}{E_{act}}, \quad (29)$$

where $\Delta V_{eff}^{\ddagger} = A_r \Delta x_{eff}^{\ddagger}$, is an effective activation volume. An analogous equation written as a function of P is:

$$E_{act}(P) = E_{act} + \alpha(r)\mu P\Delta V_{eff}^{\ddagger} + \beta(r)\frac{\left(\mu P\Delta V_{eff}^{\ddagger}\right)^2}{E_{act}}. \quad (30)$$

The activation energy in the absence of a force provides information on the thermal reaction rate for the tribochemical process and can be directly compared with the rate constant for the thermal reaction. Alternatively, if the tribochemical reaction is carried out as a function of temperature, a customary Arrhenius plot of $\ln(k_0)$ versus $1/T$ will yield an activation energy directly from the slope and can be compared with the activation energy for the thermal reaction. Agreement between the two values will imply that the shear-induced reaction proceeds via the lowest energy pathway and suggest that the shear force is aligned approximately along the reaction coordinate.

In principle, the analysis of the results of tribochemical reaction rates involves fitting Eqs. 29 or 30 to the experimental data of $k(\sigma)$ or $k(P)$, where the rate constant $k(\sigma(P)) = A\exp\left(-\frac{E_{act}(\sigma(P))}{k_B T}\right)$ and thus requires a value of the pre-exponential factor A. This value is often not known, unless the experiments were carried out as a function of temperature, although a "standard" value of $\frac{k_B T}{h} \sim 10^{13}$ s^{-1}, where h is Planck's constant, is often assumed for first-order reactions, based on the assumption that the partition functions in the initial and transition states are identical. In addition, tribochemical experiments are carried out for systems that have sufficiently large thermal barriers that the reaction rate in the absence of an external force is negligible. This implies that sufficiently large stresses must be applied to be able to observe any reaction so that initial changes in reaction rate with low forces will be difficult to measure. This may be an issue for potentials with sharp initial or transitions states (large $|r|$) where there is an initial nonlinear variation of $E_{act}(F)$, that then becomes linear (Fig. 5). However, in general for systems that display a Hammond effect, the results are taken to follow:

$$E_{act}(\sigma) = E_{act} + A\sigma + B\sigma^2, \quad (31)$$

where $A = \alpha(r)\Delta V_{eff}^{\ddagger}$ and $B = \beta(r)\frac{\left(\Delta V_{eff}^{\ddagger}\right)^2}{E_{act}}$. Thus, $\frac{B}{A^2} = \frac{\beta(r)}{\alpha^2(r)E_{act}}$ and can initially be used to estimate values of r. A plot of $\beta(r)/\alpha^2(r)$ is shown as a function of r in Fig. 7,

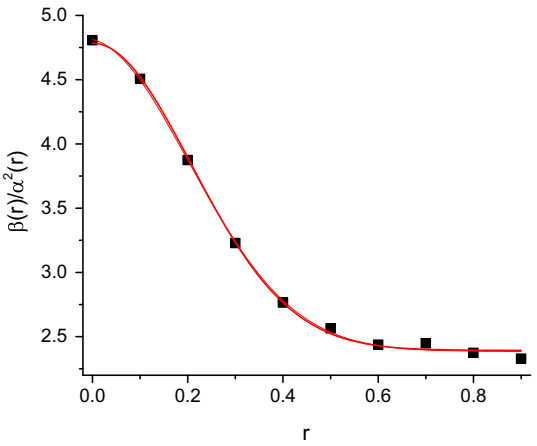

Fig. 7 Plot of the value of $\beta(r)/\alpha^2(r)$ versus r obtained from the data shown in Fig. 6

where the values are taken from the plot shown in Fig. 6. Again, the lack of good quadratic fits for large r values (Fig. 5) suggests that the results for larger values of r will be less reliable. The resulting value of r can then be used to estimate $\Delta V_{eff}^{\ddagger}$.

7.2 Analysis of Existing Tribochemical Data

In the following, these ideas are applied to analysing the existing (currently rather scant) experimental data for which shear-induced effects have been unequivocally identified and the rates measured either as a function of shear stress [23, 24] or contact pressure [21]. The rate of decomposition of adsorbates on oxygenated graphene has been measured using an AFM, where the kinetics were followed by measuring the change in friction force as a function of time [24]. The shear-induced film formation from zinc dialkyl dithiophosphate (ZDDP) was studied either by using an AFM [21] or by exerting a shear force using a viscous fluid [23], where the reaction rates were measured directly from the rate of film growth.

7.3 Application to Shear-Induced Reaction of Oxygenated Graphene

The rate of shear-induced decomposition of adsorbates formed by oxidation of graphene was studied as a function of shear stress by AFM. Here, the kinetics were followed by measuring the change in friction force during rubbing [24]. In order to compare with the above analyses, rather than plot the stress-induced reaction rate directly versus shear stress, the rate constants are converted to an activation energy $E_{act}(\sigma)$ by assuming a typical pre-exponential factor of $A = 10^{13}$ s^{-1}. The results are displayed in Fig. 8. This plot emphasizes the difficulty with analysing

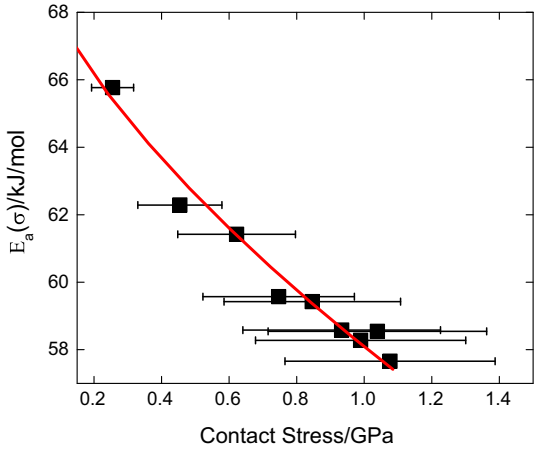

Fig. 8 Plot of change in activation barrier $E_a(\sigma)$ versus σ for the shear-induced decomposition of adsorbed species on oxidized graphene measured during sliding by an AFM. The *line* is a fit to the data for a numerical solution of the R–P potential with $r = 0.8$. Reprinted by permission from Macmillan Publishers Ltd, [24]

tribochemical kinetics using the models outlined above. The data points show a systematic curvature, consistent with the existence of a Hammond effect described above. However, the difficulty of accurately measuring the contact area leads to large uncertainties in the measured values of shear stress. Nevertheless, the scatter of the data is much lower than indicated by the error bars so that the data will be analysed by using Eq. 31 ($E_{\rm act}(\sigma) = E_{\rm act} + A\sigma + B\sigma^2$).

A fit to the data in Fig. 8 yields: $E_a(\sigma) = 69.9 \pm 0.9 - (19 \pm 3)\sigma + (7 \pm 2)\sigma^2$. The thermal activation barrier $E_a = 69.9 \pm 0.9$ kJ/mol, is in good agreement with the value of 0.73 ± 0.06 eV (70 ± 6 kJ/mol) obtained by Felts et al. [24], suggesting that the typical value of pre-exponential factor used above is reasonable. Substituting these values gives $\frac{\beta(r)}{\alpha^2(r)} = 2.0 \pm 0.6$. The results in Fig. 7 indicate that this corresponds to a value of r greater than $\sim$ 0.5, which is the region for which the fit is the least reliable. The results do, nevertheless, suggest that either the initial or transition state for the mechanically induced reaction is relatively sharp. In order to provide a more accurate estimate of $\Delta V^{\ddagger}_{\rm eff}$, the experimental data we fit to numerical solutions for the R-P potential for various values of $r > 0.5$ while adjusting the value of $\Delta V^{\ddagger}_{\rm eff}$. This yielded the best fits for $r = 0.8 \pm 0.1$ with $\Delta V^{\ddagger}_{\rm eff} = 5 \pm 2 \times 10^{-29}$ m^3, and the fit is shown as a solid line in Fig. 8. The reaction energy profile is predicted to be similar in shape to that shown in Fig. 1. A_r can be estimated using a carbon–carbon distance of 0.142 nm on graphene [63] and by taking an oxygen content of 10.9% ($\Theta = 0.109$), which yields $A_r \sim 2.3 \times 10^{-19}$ m^2. This leads to a physically reasonable value of $\Delta x^{\ddagger}_{\rm eff} = 2.2 \pm 0.9$ Å, compared to the height of the tribochemically removed layer of $\sim$ 3.7 Å. The relatively large value of $\Delta x^{\ddagger}_{\rm eff}$ compared to the length of the bond suggests that pressure effects, as discussed in Sect. 5.2, contribute to the tribochemical decomposition of adsorbates. The results also indicate that the reaction is occurring because of a strong Hammond effect that causes the initial state of the reactant to move rapidly towards the transitions state (see Fig. 1).

7.4 Application to Shear-Induced Reaction of ZDDP

The shear-induced rate of film growth from zinc dialkyl dithiophosphate (ZDDP) has recently been measured in two completely different ways, first as a function of contact pressure P using AFM [21] and as a function of shear stress using a high-viscosity fluid to avoid direct contact between the two surfaces, which was separated by a fluid film [23].

In the case of the AFM experiments, the film growth activation energy was measured separately by varying the sample temperature to yield a value of 71 $\pm$ 9 kJ/mol. The value of $E_{act}(P)$, obtained by using a standard pre-exponential factor of 1×10^{13} s^{-1} is plotted versus the contact pressure P in Fig. 9a. The activation barrier decreases rapidly up to a contact pressure of $\sim$5 GPa to a value of $\sim$53 kJ/mol, but decreases more slowly thereafter. This behaviour has been ascribed either to the onset of wear that limits the film growth rate [21] or to the influence of the formation of pads on the mechanical properties of the growing film [23]. The initial variation in activation energy with contact pressure is relatively linear. However, as noted previously, tribochemical kinetic measurements must be made for reactants that have a negligible reaction rate at the temperature at which the experiment is performed, but the increase in the stress-induced reaction rate (and the associated decrease in activation energy) must be sufficiently large for it to be measured during the experimental timescale. This can make it difficult to measure the reaction kinetics at low stresses. This is illustrated in Fig. 5, where the horizontal lines indicate the range of values of $E_{\rm act}(F)/E_{\rm act}$ corresponding to the linear region in Fig. 9a. Clearly, the variation in energy barrier versus shear stress or contact pressure over this limited range will appear linear. A linear fit to the plot of $E_{\rm act}(P)$ versus P in Fig. 9a yields: $E_{\rm act}(P) = 71.4 \pm 0.9 - (3.6 \pm 0.2)P$. The resulting value of $E_{\rm act}$ of $\sim$ 71 kJ/mol is close to that found above (71 $\pm$ 9 kJ/mol). This implies that r is less than $\sim$ 0.7, otherwise a linear extrapolation from the limited energy range to zero contact pressure would yield a lower activation barrier in Fig. 5. However, this does emphasize the

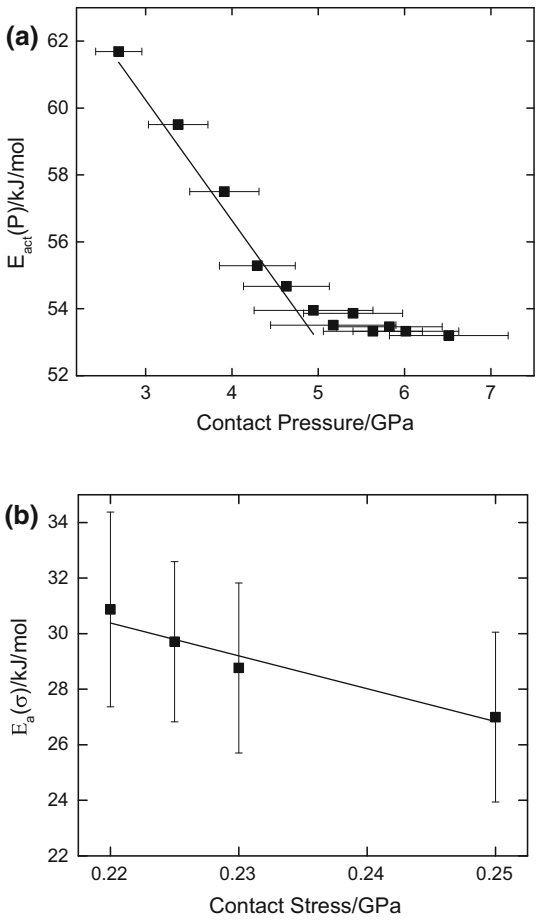

Fig. 9 Plot of change in activation barrier for tribofilms formation from ZDDP showing (**a**): a plot of $E_{\mathrm{act}}(P)$ versus P for the shear-induced film formation from ZDDP measured during sliding by an AFM (From [21]. Reprinted with permission from AAAS) and (**b**): a plot of $E_{\mathrm{act}}(\sigma)$ versus σ for the shear-induced film formation from ZDDP in a fluid film (adapted from [23])

importance of carrying out experiments over as wide a range of contact conditions as possible and of the potential difficulties of relating tribochemical results to thermal reaction data.

Equation 30 shows that the slope of a plot of $E_{\mathrm{act}}(P)$ versus P is equal to $\alpha(r)\mu P\Delta V^{\ddagger}_{\mathrm{eff}}$, which from the linear fit to the data in Fig. 9a is equal to 3.6 ± 0.2. The corresponding quadratic term in Eq. 30, $\beta(r)\dfrac{\left(\mu P\Delta V^{\ddagger}_{\mathrm{eff}}\right)^2}{E_{\mathrm{act}}}$ would then be 0.05 for $\beta(r) \sim 0.25$ (Fig. 6). A quadratic fit to the data in Fig. 9a gives a value of coefficient of the P^2 term of 0.15 ± 0.36 and is therefore approximately zero, consistent with the predicted value. In this case, the results obey the Bell model so that $\alpha(r)\mu\Delta V^{\ddagger}_{\mathrm{eff}} = 6.1 \pm 0.3 \times 10^{-30}$ m^3. Taking $\mu \sim 0.1$ gives $\alpha(r)\Delta V^{\ddagger} = 6.1 \pm 0.3 \times 10^{-29}$ m^3. $\alpha(r) = 0.8 \pm 0.2$ for $0 < r < 0.7$ (Fig. 6), giving $\Delta V^{\ddagger} = 8 \pm 2 \times 10^{-29}$ m^3.

Analogous results were also obtained for films formed from ZDDP by shear in a high-viscosity fluid [23], where the results are displayed in Fig. 9b, plotted on the same scale as the AFM results in Fig. 9a (with the shear stress in GPa). The data were collected over a relatively narrow range of shear stresses compared to the load range accessible in the AFM experiment so that any second-order effects are impossible to discern. However, since the data in Fig. 9a show an almost linear variation in stress-induced activation barrier with shear stress, a similar linear fit gives $E_{\mathrm{act}}(\sigma) = 56 \pm 4 - (118 \pm 20)\sigma$. The reaction activation energy is, in this case, lower than that found for the AFM data. Applying the above analysis gives $\Delta V^{\ddagger} = A_{\mathrm{r}}\Delta x^{\ddagger} = 2.0 \pm 0.3 \times 10^{-28}$ m^3, and is thus 2.5 ± 1.0 times higher than for the AFM data. Based on the fact that the experiments were carried out using completely different experimental approaches, and a friction coefficient was estimated to calculate the value of $\Delta V^{\ddagger}_{\mathrm{eff}}$ from the AFM measurements, the agreement is satisfactory. In addition, the exact nature of the ZDDP used in each experiment was not specified, so that differences in the nature of the side chain could influence the behavior and the way in which the shear stress was applied in the two experiments was completely different.

8 Conclusions

This paper analyses the effects of shear stress and normal load on the rates of tribochemical reactions of adsorbates on surfaces and explores the way in which the energy profiles are influenced by the imposition of external forces and the way that this reduces the activation energies of stress-induced chemical reactions. It is shown that the force-dependent energy barrier varies approximately as $E_{\mathrm{act}}(F) = E_{\mathrm{act}} + AF + BF^2$, where the parameters A and B depend on the shape of the energy profile, and formulae for these parameters are derived using a model R–P potential for the energy profile. The effect of sliding velocity on tribochemical reaction rates is also discussed.

These ideas are used to analyse existing experimental results previously published in the literature to illustrate how they can be used to provide insights into the shape of the potential energy surface and to estimate experiment values of A and B. The above analyses assume, for simplicity, that the force is aligned along the reaction coordinate for the thermal pathway. However, this may well not be the case, and possible effects arising from the force and reaction coordinate not being aligned are also discussed. Finally, the exact nature of the reaction pathways for systems that have hitherto been studied are not well defined. Progress in fundamentally understanding the way in which

shear and normal stresses influence chemical reaction rates will come from studying well-defined model systems. This will allow the shape of the energy barrier to be calculated using first-principles DFT calculations and thus allow stringent comparisons to be made between experimentally measured rates and theory.

Acknowledgements We thank the National Science Foundation for support of this work under Grants Numbers CMMI-1265742 and CMMI-1265594.

References

1. Mang, T., Dresel, W.: Lubricants and Lubrications. Wiley-VCH, Weinheim (2001)
2. Rudnick, L.R.: Lubricant Additives: Chemistry and Applications. M. Dekker, New York (2003)
3. Yin, Z., Kasrai, M., Fuller, M., Bancroft, G.M., Fyfe, K., Tan, K.H.: Application of soft X-ray absorption spectroscopy in chemical characterization of antiwear films generated by ZDDP part I: the effects of physical parameters. Wear **202**(2), 172–191 (1997)
4. Kajdas, C., Hiratsuka, K.: Tribochemistry, tribocatalysis, and the negative-ion-radical action mechanism. Proc. Inst. Mech. Eng. J J. Eng. **223**(6), 827–848 (2009)
5. Mosey, N.J., Woo, T.K., Kasrai, M., Norton, P.R., Bancroft, G.M., Müser, M.H.: Interpretation of experiments on ZDDP antiwear films through pressure-induced cross-linking. Tribol. Lett. **24**(2), 105–114 (2006)
6. Kotvis, P.V., Tysoe, W.T.: Surface chemistry of chlorinated hydrocarbon lubricant additives—part I: extreme-pressure tribology. Tribol. Trans. **41**(1), 117–123 (1998)
7. Blunt, T.J., Kotvis, P.V., Tysoe, W.T.: Surface chemistry of chlorinated hydrocarbon lubricant additives—part II: modeling the tribological interface. Tribol. Trans. **41**(1), 129–139 (1998)
8. Beyer, M.K., Clausen-Schaumann, H.: Mechanochemistry: the mechanical activation of covalent bonds. Chem. Rev. **105**(8), 2921–2948 (2005)
9. Boldyrev, V.V., Tkáčová, K.: Mechanochemistry of solids: past, present, and prospects. J. Mater. Synth. Process. **8**(3), 121–132 (2000)
10. Levitas, V.I.: High-pressure mechanochemistry: conceptual multiscale theory and interpretation of experiments. Phys. Rev. B **70**(18), 184118 (2004)
11. Kipp, S., Šepelák, V., Becker, K.D.: Mechanochemie: chemie mit dem Hammer. Chem. unserer Zeit **39**(6), 384–392 (2005)
12. Todres, Z.V.: Organic Mechanochemistry and its Practical Applications. Taylor & Francis, Boca Raton (2006)
13. Rosen, B.M., Percec, V.: Mechanochemistry: a reaction to stress. Nature **446**(7134), 381–382 (2007)
14. Mitchenko, S.A.: Mechanochemistry in heterogeneous catalysis. Theor. Exp. Chem. **43**(4), 211–228 (2007)
15. Konôpka, M., Turanský, R., Dubecký, M., Marx, D., Štich, I.: Molecular mechanochemistry understood at the nanoscale: thiolate interfaces and junctions with copper surfaces and clusters. J. Phys. Chem. C **113**(20), 8878–8887 (2009)
16. Craig, S.L.: Mechanochemistry: a tour of force. Nature **487**(7406), 176–177 (2012)
17. Mazyar, O.A., Xie, H., Hase, W.L.: Nonequilibrium energy dissipation at the interface of sliding model hydroxylated alpha-alumina surfaces. J. Chem. Phys. **122**(9), 094713 (2005). doi:10.1063/1.1858856
18. Blok, H.: The flash temperature concept. Wear **6**(6), 483–494 (1963)
19. Kalin, M., Vižintin, J.: Comparison of different theoretical models for flash temperature calculation under fretting conditions. Tribol. Int. **34**(12), 831–839 (2001)
20. Smith, E.H., Arnell, R.D.: A new approach to the calculation of flash temperatures in dry, sliding contacts. Tribol. Lett. **52**(3), 407–414 (2013)
21. Gosvami, N.N., Bares, J.A., Mangolini, F., Konicek, A.R., Yablon, D.G., Carpick, R.W.: Mechanisms of antiwear tribofilm growth revealed in situ by single-asperity sliding contacts. Science **348**(6230), 102–106 (2015)
22. Spikes, H.: The history and mechanisms of ZDDP. Tribol. Lett. **17**(3), 469–489 (2004)
23. Zhang, J., Spikes, H.: On the mechanism of ZDDP antiwear film formation. Tribol. Lett. **63**(2), 1–15 (2016)
24. Felts, J.R., Oyer, A.J., Hernández, S.C., Whitener Jr., K.E., Robinson, J.T., Walton, S.G., Sheehan, P.E.: Direct mechanochemical cleavage of functional groups from graphene. Nat. Commun. **6**, 6467 (2015)
25. Adams, H.L., Garvey, M.T., Ramasamy, U.S., Ye, Z., Martini, A., Tysoe, W.T.: Shear-induced mechanochemistry: pushing molecules around. J. Phys. Chem. C **119**(13), 7115–7123 (2015)
26. Adams, H., Miller, B.P., Kotvis, P.V., Furlong, O.J., Martini, A., Tysoe, W.T.: In situ measurements of boundary film formation pathways and kinetics: dimethyl and diethyl disulfide on copper. Tribol. Lett. **62**(1), 1–9 (2016)
27. Jacobs, T.D.B., Carpick, R.W.: Nanoscale wear as a stress-assisted chemical reaction. Nat. Nanotechnol. **8**(2), 108–112 (2013)
28. Dong, Y., Li, Q., Martini, A.: Molecular dynamics simulation of atomic friction: A review and guide. J. Vac. Sci. Technol., A **31**(3), 030801 (2013)
29. Laidler, K.J.: Chemical Kinetics. McGraw-Hill, New York (1965)
30. Eyring, H.: The activated complex in chemical reactions. J. Chem. Phys. **3**(2), 107–115 (1935)
31. Hill, T.L.: Statistical Mechanics: Principles and Selected Applications. McGraw-Hill, New York (1956)
32. Henkelman, G., Uberuaga, B.P., Jonsson, H.: A climbing image nudged elastic band method for finding saddle points and minimum energy paths. J. Chem. Phys. **113**(22), 9901–9904 (2000)
33. Henkelman, G., Jónsson, H.: Improved tangent estimate in the nudged elastic band method for finding minimum energy paths and saddle points. J. Chem. Phys. **113**(22), 9978–9985 (2000)
34. Duwez, A.-S., Cuenot, S., Jerome, C., Gabriel, S., Jerome, R., Rapino, S., Zerbetto, F.: Mechanochemistry: targeted delivery of single molecules. Nat. Nanotechnol. **1**(2), 122–125 (2006)
35. Bailey, A., Mosey, N.J.: Prediction of reaction barriers and force-induced instabilities under mechanochemical conditions with an approximate model: a case study of the ring opening of 1,3-cyclohexadiene. J. Chem. Phys. **136**(4), 044102–044111 (2012)
36. James, S.L., Adams, C.J., Bolm, C., Braga, D., Collier, P., Friscic, T., Grepioni, F., Harris, K.D.M., Hyett, G., Jones, W., Krebs, A., Mack, J., Maini, L., Orpen, A.G., Parkin, I.P., Shearouse, W.C., Steed, J.W., Waddell, D.C.: Mechanochemistry: opportunities for new and cleaner synthesis. Chem. Soc. Rev. **41**(1), 413–447 (2012)
37. Ribas-Arino, J., Marx, D.: Covalent mechanochemistry: theoretical concepts and computational tools with applications to molecular nanomechanics. Chem. Rev. **112**(10), 5412–5487 (2012)
38. Makarov, D.E.: Perspective: mechanochemistry of biological and synthetic molecules. J. Chem. Phys. **144**(3), 030901 (2016)
39. Spikes, H., Tysoe, W.: On the commonality between theoretical models for fluid and solid friction, wear and tribochemistry. Tribol. Lett. **59**(1), 1–14 (2015)

40. Bell, G.: Models for the specific adhesion of cells to cells. Science **200**(4342), 618–627 (1978)
41. Konda, S.S.M., Brantley, J.N., Bielawski, C.W., Makarov, D.E.: Chemical reactions modulated by mechanical stress: extended Bell theory. J. Chem. Phys. **135**(16), 164103–164108 (2011)
42. Eyring, H.: Viscosity, plasticity, and diffusion as examples of absolute reaction rates. J. Chem. Phys. **4**(4), 283–291 (1936)
43. Kauzmann, W., Eyring, H.: The viscous flow of large molecules. J. Am. Chem. Soc. **62**(11), 3113–3125 (1940)
44. Evans, M.G., Polanyi, M.: Some applications of the transition state method to the calculation of reaction velocities, especially in solution. Trans. Faraday Soc. **31**, 875–894 (1935)
45. Gibbs, G.B.: The thermodynamics of thermally-activated dislocation glide. Phys. Status Solidi B **10**(2), 507–512 (1965)
46. Hirth, J.P., Nix, W.D.: An analysis of the thermodynamics of dislocation glide. Phys. Status Solidi B **35**(1), 177–188 (1969)
47. Kocks, U.F., Argon, A.S., Ashby, M.F.: Thermodynamics and kinetics of slip. Prog. Mater Sci. **19**, 280 (1975)
48. Gibbs, G.B.: On the interpretation of experimental activation parameters for dislocation glide. Philos. Mag. **20**(166), 867–872 (1969)
49. Taylor, G.: Thermally-activated deformation of BCC metals and alloys. Prog. Mater Sci. **36**, 29–61 (1992)
50. Marcus, R.A.: On the theory of oxidation-reduction reactions involving electron transfer. J. Chem. Phys. **24**(5), 966–978 (1956)
51. Hammond, G.S.: A correlation of reaction rates. J. Am. Chem. Soc. **77**(2), 334–338 (1955)
52. Hyeon, C., Thirumalai, D.: Forced-unfolding and force-quench refolding of RNA hairpins. Biophys. J. **90**(10), 3410–3427 (2006)
53. Remoissenet, M., Peyrard, M.: A new simple model of a kink bearing Hamiltonian. J. Phys. C Solid State **14**(18), L481 (1981)
54. Prandtl, L.: Ein Gedankenmodell zur kinetischen Theorie der festen Körper. Z. Angew. Math. Mech. **8**, 85 (1928)
55. Furlong, O.J., Manzi, S.J., Pereyra, V.D., Bustos, V., Tysoe, W.T.: Monte Carlo simulations for Tomlinson sliding models for non-sinusoidal periodic potentials. Tribol. Lett. **39**(2), 177–180 (2010)
56. Konda, S.S.M., Brantley, J.N., Varghese, B.T., Wiggins, K.M., Bielawski, C.W., Makarov, D.E.: Molecular catch bonds and the anti-Hammond effect in polymer mechanochemistry. J. Am. Chem. Soc. **135**(34), 12722–12729 (2013)
57. Prezhdo, O.V., Pereverzev, Y.V.: Theoretical aspects of the biological catch bond. Acc. Chem. Res. **42**(6), 693–703 (2009)
58. Sokurenko, E.V., Vogel, V., Thomas, W.E.: Catch-bond mechanism of force-enhanced adhesion: counterintuitive, elusive, but … widespread? Cell Host Microbe **4**(4), 314–323 (2008)
59. Riedo, E., Gnecco, E., Bennewitz, R., Meyer, E., Brune, H.: Interaction potential and hopping dynamics governing sliding friction. Phys. Rev. Lett. **91**(8), 084502 (2003)
60. Pastewka, L., Moser, S., Gumbsch, P., Moseler, M.: Anisotropic mechanical amorphization drives wear in diamond. Nat. Mater. **10**(1), 34–38 (2011)
61. Li, Q., Tullis, T.E., Goldsby, D., Carpick, R.W.: Frictional ageing from interfacial bonding and the origins of rate and state friction. Nature **480**(7376), 233–236 (2011)
62. Mikulski, P.T., Gao, G., Chateauneuf, G.M., Harrison, J.A.: Contact forces at the sliding interface: mixed versus pure model alkane monolayers. J. Chem. Phys. **122**(2), 024701–024709 (2005)
63. Pozzo, M., Alfè, D., Lacovig, P., Hofmann, P., Lizzit, S., Baraldi, A.: Thermal expansion of supported and freestanding graphene: lattice constant versus interatomic distance. Phys. Rev. Lett. **106**(13), 135501 (2011)